Ab Initio Electronic Structure Calculations by Auxiliary-Field Quantum Monte Carlo

7

Shiwei Zhang

Contents

Abstract

The auxiliary-field quantum Monte Carlo (AFQMC) method provides a computational framework for solving the time-independent Schrödinger equation in atoms, molecules, solids, and a variety of model systems by stochastic sampling. We introduce the theory and formalism behind this framework, briefly discuss the key technical steps that turn it into an effective and practical computational method, present several illustrative results, and conclude with comments on the prospects of ab initio computation by this framework.

S. Zhang (✉)
Center for Computational Quantum Physics, Flatiron Institute, New York, NY, USA

Department of Physics, College of William and Mary, Williamsburg, VA, USA
e-mail: szhang@flatironinstitute.org

W. Andreoni, S. Yip (eds.), *Handbook of Materials Modeling*,
https://doi.org/10.1007/978-3-319-44677-6_47

1 Introduction

Predicting materials properties requires robust and reliable calculations at the most fundamental level. Often the effects being studied or designed originate from electron correlations, and small errors in their treatment can result in crucial and qualitative differences in the properties. The accurate treatment of interacting quantum systems is one of the grand challenges in modern science. In condensed phase materials, the challenge is increased by the need to account for the interplay between the electrons and the chemical and structural environment. Progress in addressing this challenge will be fundamental to achieving the materials genome initiative.

Explicit solution of the many-body Schrödinger equation leads to rapidly growing computational cost as a function of system size (see, e.g., Szabo and Ostlund 1989). To circumvent the problem, most computational quantum mechanical studies of large, realistic systems rely on simpler independent-particle approaches based on density-functional theory (DFT) (see, e.g., Kohn 1999; Martin 2004), using an approximate energy functional to include many-body effects. These replace the electron-electron interaction by an effective potential, thereby reducing the problem to a set of one-electron equations. Methods based on DFT and through its Car-Parrinello molecular dynamics implementation (Car and Parrinello 1985) have been extremely effective in complex molecules and solids (Kohn 1999). Such approaches are the standard in electronic structure, widely applied in condensed matter, quantum chemistry, and materials science.

Despite the tremendous successes of DFT, the treatment of electronic correlation is approximate. For strongly correlated systems (e.g., high-temperature superconductors, heavy-fermion metals, magnetic materials, optical lattices), where correlation effects from particle interaction crucially modify materials properties, the approximation can lead to qualitatively incorrect results. Even in moderately correlated systems when the method is qualitatively correct, the results are sometimes not sufficiently accurate. For example, in ferroelectric materials the usually acceptable 1% errors in DFT predictions of the equilibrium lattice constant can lead to almost full suppression of the ferroelectric order.

The development of alternatives to independent-particle theories is therefore of paramount fundamental and practical significance. To accurately capture the quantum many-body effects, the size of the Hilbert space involved often grows exponentially. Simulation methods utilizing Monte Carlo (MC) sampling (Kalos et al. 1974; Foulkes et al. 2001; Ceperley 1995; Blankenbecler et al. 1981; Sugiyama and Koonin 1986; Zhang and Krakauer 2003) are, in principle, both non-perturbative and well-equipped to handle details and complexities in the external environment. They are a unique combination of accuracy, general applicability, favorable scaling (low-power) for computational cost with physical system size, and scalability on parallel computing platforms (Esler et al. 2008).

For fermion systems, however, a so-called "sign" problem (Schmidt and Kalos 1984; Loh et al. 1990; Zhang 1999a) arises in varying forms in these MC simulation methods. The Pauli exclusion principle requires that the states be antisymmetric

under interchange of two particles. As a consequence, negative signs appear, which cause cancelations among contributions of the MC samples of the wave function or density matrix. In some formalism, as discussed below, a phase appears which leads to a continuous degeneracy and more severe cancelations. As the temperature is lowered or the system size is increased, such cancelation becomes more and more complete. The net signal thus decays *exponentially* versus noise. The algebraic scaling is then lost, and the method breaks down. Clearly the impact of this problem on the study of correlated electron systems is extremely severe.

In this chapter, we discuss the auxiliary-field quantum Monte Carlo (AFQMC) method for many-body computations in real materials. We cast the MC random walks in a space of over-complete Slater determinants, which significantly reduce the severity of the sign problem. In this space we formulate constraints on the random walk paths which lead to better approximations that are less sensitive to the details of the constraint. We then develop internal checks and constraint release methods to systematically improve the approach. These methods have come under the name of constrained path Monte Carlo (CPMC) (Zhang et al. 1997) for systems where there is a sign problem (e.g., Hubbard-like models where the auxiliary fields are real due to the short-ranged interactions). For electronic systems where there is a phase problem (as the Coulomb interaction leads to complex fields), the methods have been referred to as phaseless AFQMC (Zhang and Krakauer 2003; Al-Saidi et al. 2006; Motta and Zhang 2018). Here we will refer to the method as AFQMC; when necessary to emphasize the constrained-path (CP) approximation to distinguish the method from unconstrained free-projection, we will refer to it as CP-AFQMC.

2 Formalism

The Hamiltonian for any many-fermion system with two-body interactions (e.g., the electronic Hamiltonian under the Born-Oppenheimer approximation) can be written as

$$\hat{H} = \hat{H}_1 + \hat{H}_2 = -\frac{\hbar^2}{2m}\sum_{m=1}^{M}\nabla_m^2 + \sum_{m=1}^{M} V_{\text{ext}}(\mathbf{r}_m) + \sum_{m<n}^{M} V_{\text{int}}(\mathbf{r}_m - \mathbf{r}_n)\,, \tag{1}$$

where $\mathbf{r}_m$ is the real-space coordinate of the m-th fermion. The one-body part of the Hamiltonian, $\hat{H}_1$, consists of the kinetic energy of the electrons and the effect of the ionic (and any other external) potentials. (We have represented the external potential as local, although this does not have to be the case. For example, in plane-wave calculations, we will use a norm-conserving pseudopotential, which will lead to a nonlocal function V_{ext}.) The two-body part of the Hamiltonian, $\hat{H}_2$, contains the electron-electron interaction terms. The total number of fermions, M, will be fixed in the calculations we discuss. For simplicity, we have suppressed spin-index, but the spin will be made explicit when necessary. In that case, M_σ is the number

of electrons with spin σ ($\sigma = \uparrow$ or $\downarrow$). We assume that the interaction is spin-independent, so the total S_z, defined by $(M_\uparrow - M_\downarrow)$, is fixed in the calculation, although it will be straightforward to generalize our discussions to treat other cases, for example, when there is spin-orbit coupling (SOC) (Rosenberg et al. 2017).

With any chosen one-particle basis, the Hamiltonian can be written in second quantization in the general form

$$\hat{H} = \hat{H}_1 + \hat{H}_2 = \sum_{i,j}^{N} T_{ij} c_i^\dagger c_j + \frac{1}{2} \sum_{i,j,k,l}^{N} V_{ijkl} c_i^\dagger c_j^\dagger c_k c_l \,, \tag{2}$$

where the one-particle basis, $\{|\chi_i\rangle\}$ with $i = 1, 2, \cdots, N$, can be lattice sites (Hubbard model), plane waves (as in solid state calculations) (Suewattana et al. 2007), Gaussians (as in quantum chemistry) (Al-Saidi et al. 2006; Purwanto et al. 2011), etc. The operators $c_i^\dagger$ and c_i are creation and annihilation operators on $|\chi_i\rangle$, satisfying standard fermion commutation relations. The one-body matrix elements, T_{ij}, contain the effect of both the kinetic energy and external potential, while the two-body matrix elements, V_{ijkl}, are from the interaction. The matrix elements are expressed in terms of the basis functions, for example,

$$V_{ijkl} = \int d\mathbf{r}_1 d\mathbf{r}_2 \chi_i^*(\mathbf{r}_1) \chi_j^*(\mathbf{r}_2) V_{\text{int}}(\mathbf{r}_1 - \mathbf{r}_2) \chi_k(\mathbf{r}_2) \chi_l(\mathbf{r}_1) \,. \tag{3}$$

In quantum chemistry calculations, these are readily evaluated with standard Gaussian basis sets. In solid state calculations with plane waves, the kinetic and electron-electron interaction terms have simple analytic expressions, while the electron-ion potential leads to terms which are provided by the pseudopotential generation. We will assume that all matrix elements in Eq. (2) have been evaluated and are known as we begin our many-body calculations.

2.1 Non-orthogonal Slater Determinant Space

The AFQMC method seeks to obtain the ground state of the Hamiltonian in Eq. (2), representing it stochastically in the form

$$|\Psi_0\rangle = \sum_\phi \alpha_\phi |\phi\rangle \,, \tag{4}$$

where $|\phi\rangle$ is a Slater determinant:

$$|\phi\rangle \equiv \hat{\varphi}_1^\dagger \hat{\varphi}_2^\dagger \cdots \hat{\varphi}_M^\dagger |0\rangle \,. \tag{5}$$

In Eq. (5), the operator $\hat{\varphi}_m^\dagger \equiv \sum_i c_i^\dagger \varphi_{i,m}$, with m taking an integer value among $1, 2, \cdots, M$, creates an electron in a single-particle orbital φ_m: $\hat{\varphi}_m^\dagger |0\rangle = \sum_i \varphi_{i,m} |\chi_i\rangle$. The content of the orbital can thus be conveniently expressed as an

N-dimensional vector $\{\varphi_{1,m}, \varphi_{2,m}, \cdots, \varphi_{N,m}\}$. The Slater determinant $|\phi\rangle$ in Eq. (5) can then be expressed as an $N \times M$ matrix:

$$\Phi \equiv \begin{pmatrix} \varphi_{1,1} & \varphi_{1,2} & \cdots & \varphi_{1,M} \\ \varphi_{2,1} & \varphi_{2,2} & \cdots & \varphi_{2,M} \\ \vdots & \vdots & & \vdots \\ \varphi_{N,1} & \varphi_{N,2} & \cdots & \varphi_{N,M} \end{pmatrix}.$$

Each column of this matrix represents a single-particle orbital that is completely specified by its N-dimensional vector. For convenience, we will think of the different columns as all properly orthonormalized, which is straightforward to achieve by, for example, modified Gram-Schmidt (see e.g., Zhang 2003, 2013; Motta and Zhang 2018).

The mean-field Hartree-Fock (HF) solution is of course an example of a Slater determinant: $|\phi_{\mathrm{HF}}\rangle = \prod_\sigma |\phi^\sigma_{\mathrm{HF}}\rangle$, where $|\phi^\sigma_{\mathrm{HF}}\rangle$ is defined by a matrix $\Phi^\sigma_{\mathrm{HF}}$ whose columns are the M_σ lowest HF eigenstates. Similarly, the occupied manifold in a DFT calculation forms a "wave function" which is a Slater determinant.

In standard quantum chemistry (QC) methods, the many-body ground-state wave function is also represented by a sum of Slater determinants. However, there is a key difference between it and the AFQMC representation. In QC methods, the different Slater determinants are orthogonal. As illustrated in the left panel in Fig. 1, each of the determinants is formed by excitations from the HF determinant. In other words, each $|\phi\rangle$ on the right-hand side of Eq. (4) is given by a set of M molecular orbitals (MOs), and the corresponding matrix is formed by orthonormal *unit vectors*. In contrast, in AFQMC the different Slater determinants on the right-hand side of Eq. (4) are not orthogonal: $\langle\phi'|\phi\rangle \neq 0$. They are obtained by rotations of the occupied orbitals using one-body Hamiltonians involving random auxiliary fields (see further details below), as illustrated in the right panel in Fig. 1.

Several properties of non-orthogonal Slater determinants are worth mentioning. The overlap between two of them is given by

$$\langle\phi|\phi'\rangle = \det\left(\Phi^\dagger \Phi'\right). \tag{6}$$

We can define the expectation of an operator $\hat{O}$ with respect to a pair of non-orthogonal Slater determinants:

$$\langle\hat{O}\rangle_{\phi\phi'} \equiv \frac{\langle\phi|\hat{O}|\phi'\rangle}{\langle\phi|\phi'\rangle}, \tag{7}$$

for instance, single-particle Green's function $G_{ij} \equiv \langle c_i c_j^\dagger\rangle_{\phi\phi'}$:

$$G_{ij} \equiv \frac{\langle\phi|c_i c_j^\dagger|\phi'\rangle}{\langle\phi|\phi'\rangle} = \delta_{ij} - [\Phi'(\Phi^\dagger\Phi')^{-1}\Phi^\dagger]_{ij}. \tag{8}$$

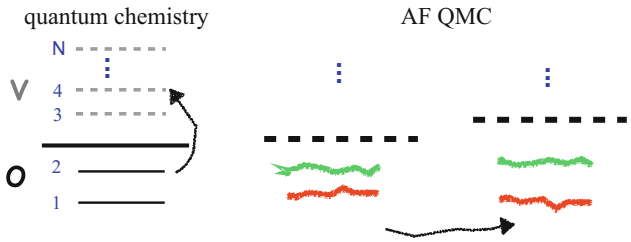

Fig. 1 Schematic illustration of the connection and difference between quantum chemistry (QC) approaches and AFQMC. A fictitious system, with $M_\uparrow = 2$, $M_\downarrow \leq M_\uparrow$ and N basis functions, is shown. Vertical scale indicates single-particle energy. In QC-based methods (left), Slater determinants are constructed using the molecular orbitals from a (restricted-orbital) HF calculation. ("O" denotes occupied, "V" denotes virtual, and the thick line indicates the Fermi level.) All resulting Slater determinants are orthogonal to each other and to the reference HF state. In AFQMC, each Slater determinant in Eq. (4) is sampled by random walk. Each walker $|\phi\rangle$ has only "occupied" orbitals (denoted by the red and green lines) which are rotated during the random walk, under the influence of stochastic auxiliary fields (illustrated by the *wiggly* lines, which move up and down as the walker evolves from one step to the next). The Slater determinants generated in AFQMC are non-orthogonal to each other

Given the Green's function matrix G, the general expectation defined in Eq. (7) can be computed for most operators of interest. For example, we can calculate the expectation of a general two-body operator, $\hat{O} = \sum_{ijkl} O_{ijkl} c_i^\dagger c_j^\dagger c_k c_l$, under the definition of Eq. (7):

$$\langle \hat{O} \rangle_{\phi\phi'} = \sum_{ijkl} O_{ijkl} (G'_{jk} G'_{il} - G'_{ik} G'_{jl}), \tag{9}$$

where the matrix G' is defined as $G' \equiv I - G$.

A key property of Slater determinants we will invoke is the *Thouless Theorem*: any one-particle operator $\hat{B}$ of the form

$$\hat{B} = \exp\left(\sum_{ij} c_i^\dagger U_{ij} c_j \right), \tag{10}$$

when acted on a Slater determinant, simply leads to another Slater determinant (Hamann and Fahy 1990), i.e.,

$$\hat{B}|\phi\rangle = \hat{\phi}_1'^\dagger \hat{\phi}_2'^\dagger \cdots \hat{\phi}_M'^\dagger |0\rangle \equiv |\phi'\rangle \tag{11}$$

with $\hat{\phi}_m'^\dagger = \sum_j c_j^\dagger \Phi'_{jm}$ and $\Phi' \equiv e^U \Phi$, where U is a square matrix whose elements are given by U_{ij} and $B \equiv \exp(U)$ is therefore an $N \times N$ square matrix as well. In other words, the operation of $\hat{B}$ on $|\phi\rangle$ simply involves multiplying an $N \times N$ matrix to the $N \times M$ matrix representing the Slater determinant.

There are several generalizations of the formalism we have discussed which extends the capability and/or accuracy of the AFQMC framework. These can be thought of as generalizing one or both of the Slater determinants in Eqs. (6), (7), and (8). From the viewpoint of AFQMC, as we shall discuss below, the"bra" in these equations represents the trial wave function, and the "ket" represents the random walker:

- The first generalization is to replace $\langle\phi|$ by a projected Bardeen-Cooper-Schrieffer (BCS) wave function, that is, to use a projected BCS as a trial wave function, which can be advantageous for systems with pairing order. The corresponding overlap, Green functions, and two-body mixed expectations have been worked out (Carlson et al. 2011).
- The second is to have both $\langle\phi|$ and $|\phi'\rangle$ in generalized HF (GHF) form, which is necessary to treat systems with spin-orbit coupling (SOC). The required modification to the formalism outlined above is given by Rosenberg et al. (2017).
- The third generalization is to have both sides in Hartree-Fock-Bogoliubov (HFB) form, for example, to treat Hamiltonians with pairing fields. This will also be useful when using AFQMC as an impurity solver in which the embedding induces pairing order. The corresponding AFQMC formalism has been described (Shi and Zhang 2017).

2.2 Ground-State Projection

Most ground-state quantum MC (QMC) methods are based on iterative projection:

$$|\Psi_0\rangle \propto \lim_{\tau\to\infty} e^{-\tau\hat{H}}|\Psi_T\rangle; \tag{12}$$

that is, the ground state $|\Psi_0\rangle$ of a many-body Hamiltonian $\hat{H}$ can be projected from any known trial state $|\Psi_T\rangle$ that satisfies $\langle\Psi_T|\Psi_0\rangle \neq 0$. In a numerical method, the limit can be obtained iteratively by

$$|\Psi^{(n+1)}\rangle = e^{-\Delta\tau\hat{H}}|\Psi^{(n)}\rangle, \tag{13}$$

where $|\Psi^{(0)}\rangle = |\Psi_T\rangle$. Ground-state expectation $\langle\hat{O}\rangle$ of a physical observable $\hat{O}$ is given by

$$\langle\hat{O}\rangle = \lim_{n\to\infty} \frac{\langle\Psi^{(n)}|\hat{O}|\Psi^{(n)}\rangle}{\langle\Psi^{(n)}|\Psi^{(n)}\rangle}. \tag{14}$$

For example, the ground-state energy can be obtained by letting $\hat{O} = \hat{H}$. A so-called mixed estimator exists, however, which is exact for the energy (or any other $\hat{O}$ that commutes with $\hat{H}$) and can lead to considerable simplifications in practice:

$$E_0 = \lim_{n\to\infty} \frac{\langle \Psi_T | \hat{H} | \Psi^{(n)} \rangle}{\langle \Psi_T | \Psi^{(n)} \rangle}. \tag{15}$$

QMC methods carry out the iteration in Eq. (13) by Monte Carlo (MC) sampling. The difference between different classes of methods amounts primarily to the space that is used to represent the wave function or density matrix and to carry out the integration. The AFQMC methods work in second quantized representation and in an auxiliary-field space, while Green's function Monte Carlo (GFMC) or diffusion Monte Carlo (DMC) works in first-quantized representation and in electron coordinate space (Kalos et al. 1974; Foulkes et al. 2001). The full-configuration interaction QMC (FCIQMC) (Booth et al. 2009) works in orthogonal Slater determinant space as in QC methods.

Let us assume that $|\Psi_T\rangle$ is of the form of a single Slater determinant or a linear combination of Slater determinants, as in Eq. (4). The operation of $e^{-\tau \hat{H}_1}$ on a Slater determinant simply yields another determinant, per Thouless theorem. The ground-state projection would therefore turn into the propagation of a single Slater determinant if it were somehow possible to write the two-body propagator $e^{-\tau \hat{H}_2}$ as the exponential of a one-body operator.

The above is realized in independent-electron theories. In the HF approximation, $\hat{H}_2$ is replaced by one-body operators times expectations with respect to the current Slater determinant wave function, schematically:

$$c_i^\dagger c_j^\dagger c_k c_l \to c_i^\dagger c_l \langle c_j^\dagger c_k \rangle - c_i^\dagger c_k \langle c_j^\dagger c_l \rangle \,. \tag{16}$$

(A decomposition that includes pairing is also possible, leading to a Hartree-Fock-Bogoliubov calculation.) In the local density approximation (LDA) in DFT, $\hat{H}_2$ is replaced by $\hat{H}_{\mathrm{LDA}} = \hat{H}_1 + \hat{V}_{xc}$, where $\hat{V}_{xc}$ contains the density operator in real-space, with matrix elements given by the exchange-correlation functional which is computed with the local density from the current Slater determinant in the self-consistent process. In both these cases, an iterative procedure can be used, following Eq. (13), to project out the solution to the approximate Hamiltonians, as an imaginary-time evolution of a single Slater determinant (Zhang and Ceperley 2008). This is illustrated by the blue line in Fig. 2. Note that this procedure is formally very similar to time-dependent HF or time-dependent DFT (TDDFT), except for the distinction of imaginary versus real time.

2.3 Hubbard-Stratonovich Transformation

Suppose that $\hat{H}_2$, the two-body part in the Hamiltonian in Eq. (2), can be written as a sum of squares of one-body operators:

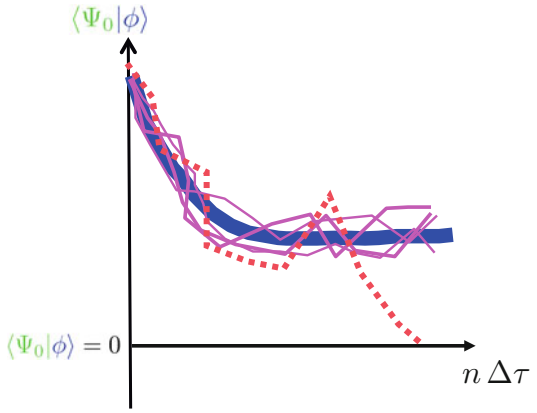

Fig. 2 Illustration of the iterative imaginary-time projection to the ground state. The overlap of the Slater determinants with a test wave function (e.g., the exact ground-state $|\Psi_0\rangle$) is plotted vs. imaginary time $n\Delta\tau$. The thick blue line indicates a projection using $e^{-\Delta\tau \hat{H}_{\mathrm{LDA}}(\phi^{(n)})}$ which converges to the LDA ground state (or a local minimum). The wiggly magenta lines indicate an AFQMC projection which captures the many-body effect beyond LDA as a stochastic linear superposition. The propagator is obtained by expanding the two-body part of the $\hat{H}$, namely, $\hat{H}_2 - \hat{V}_{xc}$, by a Hubbard-Stratonovich transformation as discussed in the next sections. The dotted redline indicates a path which can lead to a sign problem (Sect. 3.2)

$$\hat{H}_2 = \frac{1}{2}\sum_{\gamma=1}^{N_\gamma} \lambda_\gamma \hat{v}_\gamma^2, \tag{17}$$

where λ_γ is a constant, $\hat{v}_\gamma$ is a one-body operator similar to $\hat{H}_1$, and N_γ is an integer. We can then apply the Hubbard-Stratonovich (HS) transformation to each term

$$e^{-\frac{\Delta\tau}{2}\lambda\,\hat{v}^2} = \int_{-\infty}^{\infty} dx \frac{e^{-\frac{1}{2}x^2}}{\sqrt{2\pi}} e^{x\sqrt{-\Delta\tau\lambda}\,\hat{v}}, \tag{18}$$

where x is an auxiliary-field variable. The constant in front of $\hat{v}$ in the exponent on the right-hand side can be real or imaginary, depending on the sign of λ. The key is that the quadratic form (in $\hat{v}$) on the left is replaced by a linear one on the right. There are various ways to achieve the decomposition in Eq. (17) for a general two-body term (Negele and Orland 1998). Below we outline the two most commonly applied cases in electronic structure: (**a**) *with plane-wave basis* and (**b**) for a more dense matrix V_{ijkl} resulting from a *general basis set* such as Gaussians in QC.

In a *plane-wave basis*, the two-body part is the Fourier transform of $1/|\mathbf{r}_m - \mathbf{r}_n|$ (Suewattana et al. 2007):

$$\hat{H}_2 \to \frac{1}{2\Omega}\sum_{i,j,k,l} \frac{4\pi}{|\mathbf{G_i} - \mathbf{G_k}|^2} c_i^\dagger c_j^\dagger c_l c_k \delta_{\mathbf{G_i}-\mathbf{G_k},\mathbf{G_l}-\mathbf{G_j}} \delta_{\sigma_i,\sigma_k} \delta_{\sigma_j,\sigma_l}\,, \tag{19}$$

where $\{\mathbf{G_i}\}$ are plane-wave wave-vectors, Ω is the volume of the supercell, and σ denotes spin. Let us use $\mathbf{Q} \equiv \mathbf{G_i} - \mathbf{G_k}$ and define a density operator in momentum space:

$$\hat{\rho}(\mathbf{Q}) \equiv \sum_{\mathbf{G},\sigma} c^{\dagger}_{\mathbf{G}+\mathbf{Q},\sigma} c_{\mathbf{G},\sigma}, \tag{20}$$

where the sum is over all $\mathbf{G}$ vectors which allow both $\mathbf{G}$ and $\mathbf{G}+\mathbf{Q}$ to fall within the predefined kinetic energy cutoff in the plane-wave basis. The two-body term in Eq. (19) can then be manipulated into the form

$$\hat{H}_2 \rightarrow \sum_{\mathbf{Q}\neq\mathbf{0}} \frac{\pi}{\Omega Q^2} \left[\hat{\rho}^{\dagger}(\mathbf{Q})\,\hat{\rho}(\mathbf{Q}) + \hat{\rho}(\mathbf{Q})\,\hat{\rho}^{\dagger}(\mathbf{Q})\right], \tag{21}$$

where the sum is over all $\mathbf{Q}$'s except $\mathbf{Q} = 0$, since in Eq. (19) the $\mathbf{G_i} = \mathbf{G_k}$ term is excluded due to charge neutrality, and we have invoked $\rho^{\dagger}(\mathbf{Q}) = \rho(-\mathbf{Q})$. By making linear combinations of $\left[(\rho^{\dagger}(\mathbf{Q}) + \rho(\mathbf{Q})\right]$ and $\left[(\rho^{\dagger}(\mathbf{Q}) - \rho(\mathbf{Q})\right]$ terms, we can then readily write the right-hand side in Eq. (21) in the desired square form of Eq. (17) (Suewattana et al. 2007).

With a *general basis* such as Gaussians yielding matrix elements given in Eq. (3), the most straightforward way to decompose $\hat{H}_2$ is through a direct diagonalization (Al-Saidi et al. 2006, 2007; Zhang 2013). However, this is computationally costly. A modified Cholesky decomposition leads to $\mathcal{O}(N)$ fields (Purwanto et al. 2011; Motta and Zhang 2018). This approach, which has been commonly used in AFQMC for molecular systems with Gaussian basis sets and for downfolded Hamiltonians (Ma et al. 2015), proceeds as follows. Let us cast V_{ijkl} in the form of a two-index matrix by introducing the compound indices $\mu = (i,l)$ and $\nu = (j,k)$: $V_{\mu\nu} = V_{(i,l),(j,k)} = V_{ijkl}$. The symmetric positive semidefinite matrix $V_{\mu\nu}$ is decomposed using a recursive modified Cholesky algorithm (Koch et al. 2003; Aquilante et al. 2010), to yield

$$V_{\mu\nu} = \sum_{\gamma=1}^{N_\gamma} L^{\gamma}_{\mu} L^{\gamma}_{\nu} + \Delta^{(N_\gamma)}_{\mu\nu}, \tag{22}$$

where $\Delta^{(N_\gamma)}_{\mu\nu}$ is the residual error at the N_γ-th iteration. The iterative procedure is repeated until all matrix elements of the residual matrix are less than some predefined tolerance δ:

$$\left|V_{\mu\nu} - V^{(N_{\mathrm{CD}})}_{\mu\nu}\right| = \left|\Delta^{(N_{\mathrm{CD}})}_{\mu\nu}\right| \leq \delta\,. \tag{23}$$

For molecular calculations, typical values of δ range between 10^{-4} and 10^{-6} in atomic units (Motta and Zhang 2018). Using the N_{CD} Cholesky vectors, we can rewrite the two-body part of the Hamiltonian

$$\hat{H}_2 \to \frac{1}{2}\sum_{\gamma=1}^{N_{\rm CD}} \left(\sum_{il} L^{\gamma}_{\mu(i,l)} c_i^\dagger c_l\right)\left(\sum_{jk} L^{\gamma}_{\nu(j,k)} c_j^\dagger c_k\right) + \mathcal{O}(\delta)\,. \tag{24}$$

Hence the form in Eq. (17) is realized, with $\hat{v}_\gamma = \sum_{il} L^{\gamma}_{\mu(i,l)} c_i^\dagger c_l$.

Different forms of the HS transformation can affect the performance of the AFQMC method. For example, it is useful to subtract a mean-field "background" from the two-body term prior to the decomposition (Baer et al. 1998; Purwanto and Zhang 2005; Al-Saidi et al. 2006). The idea is that using the HS to decompose any constant shifts in the two-body interaction will necessarily result in more statistical noise. In fact, it has been shown (Shi and Zhang 2013; Motta and Zhang 2018) that the mean-field background subtraction can not only impact the statistical accuracy but also lead to different quality of approximations under the constrained path methods that we discuss in the next section.

If we denote the collection of auxiliary fields by $\mathbf{x}$ and combine one-body terms from $\hat{H}_1$ and $\hat{H}_2$, we obtain the following compact representation of the outcome of the HS transformation:

$$e^{-\Delta\tau \hat{H}} = \int d\mathbf{x}\, p(\mathbf{x})\, \hat{B}(\mathbf{x}), \tag{25}$$

where $p(\mathbf{x})$ is a probability density function (PDF), for example, a multidimensional Gaussian. The propagator $\hat{B}(\mathbf{x})$ in Eq. (25) has a *special form*, namely, it is a product of operators of the type in Eq. (10), with U_{ij} depending on the auxiliary field. The matrix representation of $\hat{B}(\mathbf{x})$ will be denoted by $B(\mathbf{x})$.

Note that the matrix elements of $B(\mathbf{x})$ can become complex, for example, when λ in Eq. (18) is positive, which occurs in both of the forms discussed above. Sometimes we will refer to this situation as having complex auxiliary fields, but it should be understood that terms in the PDF of the HS transformation and $\hat{B}(\mathbf{x})$ can be rearranged, and the relevant point is whether the Slater determinant has matrix elements which are real or complex, as further discussed in the next section.

In essence, the HS transformation replaces the two-body interaction by one-body interactions with a set of random external auxiliary fields. In other words, it converts an interacting system into many *noninteracting* systems living in fluctuating external auxiliary fields. The sum over all configurations of auxiliary fields recovers the interaction.

3 Ground-State AFQMC Methods

3.1 Free-Projection AFQMC

We first briefly describe the ground-state AFQMC method without any constraints. Our goal is to illustrate the essential ideas, in a way which will facilitate our ensuing discussions and help introduce the constrained path approximation and the

framework for the general AFQMC methods that control the sign/phase problem. We will not go into details, which are described in the literature.

We write the usual path-integral and Metropolis form explicitly here to show its connection to the open-ended random walk approach. Ground-state expectation $\langle \hat{O} \rangle$ can be computed with Eqs. (13) and (25). The denominator is

$$\begin{aligned} & \langle \psi^{(0)} | e^{-n\Delta\tau \hat{H}} \, e^{-n\Delta\tau \hat{H}} | \psi^{(0)} \rangle \\ &= \int \langle \psi^{(0)} | \Big[\prod_{l=1}^{2n} d\mathbf{x}^{(l)} \, p(\mathbf{x}^{(l)}) \hat{B}(\mathbf{x}^{(l)}) \Big] | \psi^{(0)} \rangle \\ &= \int \Big[\prod_{l} d\mathbf{x}^{(l)} \, p(\mathbf{x}^{(l)}) \Big] \det\Big([\Psi^{(0)}]^{\dagger} \prod_{l} B(\mathbf{x}^{(l)}) \Psi^{(0)} \Big). \end{aligned} \tag{26}$$

In the standard ground-state AFQMC method (Sugiyama and Koonin 1986; Sorella et al. 1989; Blankenbecler et al. 1981), a value of n is first chosen and is kept fixed throughout the calculation. If we use X to denote the collection of the auxiliary fields $X = \{\mathbf{x}^{(1)}, \mathbf{x}^{(2)}, \ldots, \mathbf{x}^{(2n)}\}$ and $D(X)$ to represent the integrand in Eq. (26), we can write the expectation value of Eq. (14) as

$$\langle \hat{O} \rangle = \frac{\int \langle \hat{O} \rangle_{LR} \, D(X) \, dX}{\int D(X) \, dX} = \frac{\int \langle \hat{O} \rangle_{LR} \, \big| D(X) \big| \, \Theta(X) \, dX}{\int \big| D(X) \big| \, \Theta(X) \, dX}, \tag{27}$$

where

$$\Theta(X) \equiv D(X) / \big| D(X) \big| \tag{28}$$

measures the phase of $D(X)$, which reduces to a sign when the overlap, $D(X)$, is real along all paths $\{X\}$. The expectation for a given X, as defined in Eq. (7), is:

$$\langle \hat{O} \rangle_{LR} \equiv \frac{\langle \phi_L | \hat{O} | \phi_R \rangle}{\langle \phi_L | \phi_R \rangle} \tag{29}$$

with

$$\langle \phi_L | = \langle \psi^{(0)} | \, \hat{B}(\mathbf{x}^{(2n)}) \hat{B}(\mathbf{x}^{(2n-1)}) \cdots \hat{B}(\mathbf{x}^{(n+1)})$$

$$| \phi_R \rangle = \hat{B}(\mathbf{x}^{(n)}) \hat{B}(\mathbf{x}^{(n-1)}) \cdots \hat{B}(\mathbf{x}^{(1)}) \, | \psi^{(0)} \rangle,$$

which are both Slater determinants.

$D(X)$ and $\langle \phi_L |$ and $| \phi_R \rangle$ are completely specified by the path X in auxiliary-field space, given $| \Psi^{(0)} \rangle$. The expectation in Eq. (27) is thus a many-dimensional

integration which can be evaluated by standard MC techniques. Often the Metropolis algorithm (Kalos and Whitlock 1986) is used to sample auxiliary fields X from $|D(X)|$. We will refer to this as free-projection (in contrast with a constrained path calculations). There are special Hamiltonians (e.g., repulsive Hubbard model at half-filling) where special symmetry makes the sign problem absent. In those situations, the Metropolis approach described above is very effective and is the standard approach. It should be mentioned that in those cases, an infinite variance problem arises which must be controlled (Shi and Zhang 2016).

We carry out free-projection calculations with an open-ended random walk (Zhang et al. 1997; Baer et al. 1998) instead of using Metropolis sampling outlined above. For free-projection calculations, the open-ended approach has no real advantage. However, when a sign or phase problem is present, it is difficult to implement a constraint to control the problem in the Metropolis framework, because of ergodicity issues (Fahy and Hamann 1990; Zhang et al. 1997). The open-ended random walk framework avoids the difficulty and is straightforward to project to longer imaginary time in order to approach the ground state. Moreover, when we carry out constraint release (Shi and Zhang 2013), the formalism will rely on the open-ended random walk. These points will become clear after we illustrate the phase problem in electronic structure calculations below and discuss how the constraint can be formulated. The structure of the open-ended random walk is illustrated in Fig. 3.

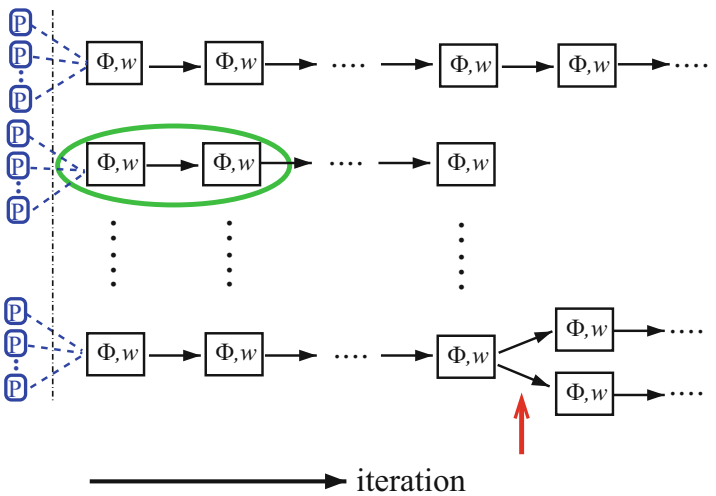

Fig. 3 Schematic illustration of the AFQMC method. Each box is a random walker, with $|\phi\rangle$ the stochastic Slater determinant and w its weight. A step (green oval) is similar to one SCF (self-consistent-field) step in LDA. The red arrow indicates a population control, where birth/death can occur. This structure allows for exceptional capacity for scaling on parallel computers. Multiple walkers can reside on one processor (blue "P" box), or each walk can be split over processors for large problems

3.2 Constrained Path AFQMC

As mentioned, a sign/phase problem occurs in the free-projection AFQMC, except for special cases where the single-particle propagator $\hat{B}(\mathbf{x})$ satisfies particular symmetries (see, e.g., Wei et al. 2016). In these cases, $\Theta(X)$ (defined in Eq. (28)) vanishes, and $D(x)$ is real and nonnegative. Absent such special circumstances, a sign problem arises if $\hat{B}(\mathbf{x})$ is real, and a phase problem arises if $\hat{B}(\mathbf{x})$ is complex. As mentioned, the Coulomb interaction in V_{int} leads to a phase problem in molecules and solids. In this section we discuss the constrained-path (CP) AFQMC, which for electronic systems has often been referred to as the phaseless or phase-free approximation (Zhang and Krakauer 2003; Purwanto and Zhang 2004).

For real $\hat{B}(\mathbf{x})$ (e.g., Hubbard-type of short-range repulsive interactions decoupled with spin form of HS transformation), the sign problem occurs because of the fundamental symmetry between the fermion ground-state $|\Psi_0\rangle$ and its negative $-|\Psi_0\rangle$ (Zhang 1999a; Zhang and Kalos 1991). For any ensemble of Slater determinants $\{|\phi\rangle\}$ which gives a MC representation of the ground-state wave function, as in Eq. (4), this symmetry implies that there exists another ensemble $\{-|\phi\rangle\}$ which is also a correct representation. In other words, the Slater determinant space can be divided into two degenerate halves ($+$ and $-$) whose bounding surface $\mathcal{N}$ is defined by $\langle\Psi_0|\phi\rangle = 0$. This dividing surface is unknown. (In the cases with special symmetry mentioned above, the two sides separated by the surface are both positive. This has to do with the over-complete nature of the non-orthogonal Slater determinant space in AFQMC. A particular form of $\hat{B}(\mathbf{x})$ can pick out only a part of the space which can be nonnegative.)

The idea of the $\pm$-symmetry can be seen from Fig. 2, where the dotted red line indicates a walker reaching the surface $\mathcal{N}$, which will have a finite probability of occurring in a random walk, unless completely excluded by the dynamics. Once it does, it can, in general, freely sample the two families of solutions which are symmetric about the horizontal axis (above and below). A more detailed illustration and discussion of the sign problem can be found in Zhang (1999b, 2013). The idea of the phase problem is illustrated in Fig. 4. The complex plane now replaces the vertical axis in Fig. 2, denoting the overlap of a random walker $|\phi\rangle$ with the (hypothetically) known exact wave function or the trial wave function $\langle\Psi_T|$.

Cancelation schemes can partially alleviate the problem, as demonstrated in coordinate space (Zhang and Kalos 1991; Diedrich and Anderson 1992) and in Fock space (Booth et al. 2009). To fully stabilize the calculation and restore polynomial scaling, however, an approximation has been necessary. To date, the most effective and accurate method to achieve this has been the constrained path approach.

The method begins with a generalized similarity transformation in the spirit of the importance-sampling transformation. To make the derivation more concrete, we will use an explicit form of the HS transformation and write the two-body propagator that results from Eq. (21) or (24) as $\int e^{-\frac{\mathbf{x}^2}{2}} e^{\mathbf{x}\cdot\hat{\mathbf{v}}} d\mathbf{x}$, where $\mathbf{x}$ is an N_γ-dimensional vector as given by Eq. (25) (with γ labeling the auxiliary fields) and

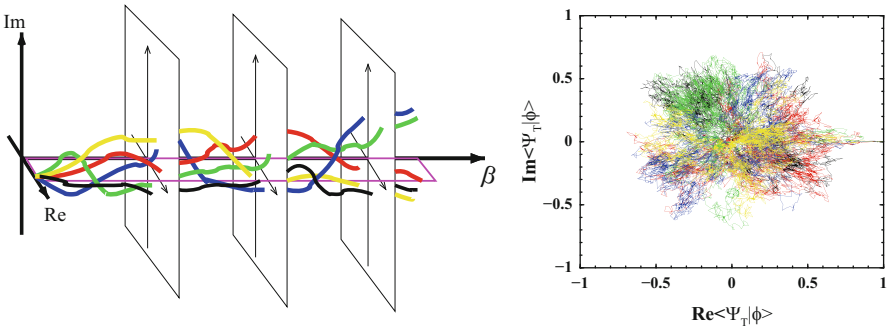

Fig. 4 Schematic illustration of the phase problem and constraints to control it. The **left panel** shows, as a function of projection time $\beta \equiv n\Delta\tau$, trajectories of five walkers (shown as five different colors) characterized by the real (Re) and imaginary (Im) parts of their overlap with the ground-state wave function. The **right panel** shows the walker distribution integrated over imaginary time, i.e., the different frames in the left panel stacked together along β. The phase problem occurs because the initial phase "coherence" of the random walkers rapidly deteriorates with β, as they become uniformly distributed in the Re-Im-plane. The idea of the phase constraint (Zhang and Krakauer 2003) is to apply a gauge transformation such that confining the random walk in the single magenta plane (left) is a good approximation

$\hat{\mathbf{v}} = \{\hat{v}_\gamma\}$ denotes the collection of one-body operators. We introduce a shift to obtain an alternative propagator:

$$\int e^{-\frac{\mathbf{x}^2}{2}} e^{\mathbf{x}\cdot\bar{\mathbf{x}}-\frac{\bar{\mathbf{x}}^2}{2}} e^{(\mathbf{x}-\bar{\mathbf{x}})\cdot\hat{\mathbf{v}}} d\mathbf{x}\,, \tag{30}$$

which is exact for any choice of the shift $\bar{\mathbf{x}}$, including complex shifts.

We recall that the random walk is supposed to lead to a MC sampling of the coefficient α_ϕ in Eq. (4):

$$|\Psi_0\rangle \doteq \sum_{\{\phi\}} w_\phi |\phi\rangle\,. \tag{31}$$

The sum in Eq. (31), which is over the population of walkers after an "equilibration" portion of the open-ended random walk has been discarded, is in a Monte Carlo sense, and is typically much smaller than the sum in Eq. (4). The weight of each walker $|\phi\rangle$, w_ϕ, can be thought of as 1 (all walkers with equal weight); it is allowed to fluctuate only for practical (efficiency) consideration.

Using the idea of importance sampling, we seek to replace Eq. (31) by the following to sample Eq. (4):

$$|\Psi_0\rangle = \sum_{\phi} w_\phi \frac{|\phi\rangle}{\langle\Psi_T|\phi\rangle}\,, \tag{32}$$

where any overall phase of the walker $|\phi\rangle$ is canceled in the numerator and denominator on the right-hand side (Zhang and Krakauer 2003). This implies a modification to the propagator in Eq. (30):

$$\int \langle \Psi_T | \phi'(\mathbf{x}) \rangle e^{-\frac{\mathbf{x}^2}{2}} e^{\mathbf{x}\bar{\mathbf{x}} - \bar{\mathbf{x}}^2/2} e^{(\mathbf{x}-\bar{\mathbf{x}})\cdot\hat{\mathbf{v}}} \frac{1}{\langle \Psi_T | \phi \rangle} d\mathbf{x}, \tag{33}$$

where $|\phi'(\mathbf{x})\rangle = e^{(\mathbf{x}-\bar{\mathbf{x}})\cdot\hat{\mathbf{v}}}|\phi\rangle$ and the trial wave function $|\Psi_T\rangle$ represents the best guess to $|\Psi_0\rangle$. Let us define the following shorthand:

$$\bar{\mathbf{v}} \equiv -\frac{\langle \Psi_T | \hat{\mathbf{v}} | \phi \rangle}{\langle \Psi_T | \phi \rangle} \sim \mathcal{O}(\sqrt{\Delta\tau}); \quad \bar{\mathbf{v}^2} \equiv \frac{\langle \Psi_T | \hat{\mathbf{v}}^2 | \phi \rangle}{\langle \Psi_T | \phi \rangle} \sim \mathcal{O}(\Delta\tau)\,. \tag{34}$$

We can then evaluate the ratio $\langle \Psi_T | \phi'(\mathbf{x}) \rangle / \langle \Psi_T | \phi \rangle$ in Eq. (33) by expanding the propagator (Moskowitz et al. 1982; Zhang and Krakauer 2003; Purwanto and Zhang 2004) to $\mathcal{O}(\tau)$, to obtain:

$$\frac{\langle \Psi_T | \phi'(\mathbf{x}) \rangle}{\langle \Psi_T | \phi \rangle} e^{\mathbf{x}\cdot\bar{\mathbf{x}} - \bar{\mathbf{x}}^2/2} \doteq \exp\left[-(\mathbf{x}-\bar{\mathbf{x}})\cdot\bar{\mathbf{v}} + \frac{1}{2}(\mathbf{x}-\bar{\mathbf{x}})^2\bar{\mathbf{v}^2} - \frac{1}{2}(\mathbf{x}-\bar{\mathbf{x}})^2\bar{\mathbf{v}}^2 + \mathbf{x}\cdot\bar{\mathbf{x}} - \bar{\mathbf{x}}^2/2 \right]. \tag{35}$$

The optimal choice of the shift $\bar{\mathbf{x}}$, which we shall refer to as a force bias, minimizes the fluctuation of Eq. (35) with respect to $\mathbf{x}$, and it is straightforward to show that it is $\bar{\mathbf{x}} = \bar{\mathbf{v}}$. With this choice, Eq. (33) can be written approximately as (Zhang 2013)

$$\int e^{-\frac{\mathbf{x}^2}{2}} e^{(\mathbf{x}-\bar{\mathbf{v}})\cdot\hat{\mathbf{v}}} e^{\frac{\bar{\mathbf{v}^2}}{2}} d\mathbf{x}. \tag{36}$$

Restoring $\hat{H}_1$, we obtain the complete propagator:

$$\int e^{-\frac{\mathbf{x}^2}{2}} \exp\left[-\frac{\Delta\tau \hat{H}_1}{2} \right] \exp\left[(\mathbf{x} - \bar{\mathbf{v}}) \cdot \hat{\mathbf{v}} \right] \exp\left[-\frac{\Delta\tau \hat{H}_1}{2} \right] \exp[-\Delta\tau E_L(\phi)]\, d\mathbf{x}, \tag{37}$$

where E_L is the local energy, the mixed estimate of the Hamiltonian:

$$E_L(\phi) \equiv \frac{\langle \Psi_T | \hat{H} | \phi \rangle}{\langle \Psi_T | \phi \rangle}. \tag{38}$$

In the limit of an exact $|\Psi_T\rangle$, E_L is a *real* constant, and the weight of each walker remains real. The mixed estimate for the energy from Eq. (15) is phaseless:

$$E_0^{\mathrm{c}} = \frac{\sum_\phi w_\phi E_L(\phi)}{\sum_\phi w_\phi}. \tag{39}$$

With a general $|\Psi_T\rangle$ which is not exact, a natural approximation is to replace E_L in Eq. (37) by its real part, $\mathrm{Re}E_L$. The same replacement is then necessary in Eq. (39).

When $\hat{B}(\mathbf{x})$ (i.e., $\hat{\mathbf{v}}$) is real, this formalism reduces to the so-called constrained-path approximation (Zhang et al. 1997). Regardless of whether $\hat{\mathbf{v}}$ is real, the shift $\bar{\mathbf{x}}$ diverges as the random walk in the complex plane (see the right panel of Fig. 4) approaches the origin, i.e., as $\langle\Psi_T|\phi'\rangle \to 0$. The effect of the divergence is to move the walker away from the origin. With a *real* $\hat{\mathbf{v}}$, the random walkers move only on the real axis. If they are initialized to have positive overlaps with $|\Psi_T\rangle$, $\bar{\mathbf{x}}$ will ensure that the overlaps remain positive throughout the random walk.

For a general case with a complex $\hat{\mathbf{v}}$, however, the formalism above by itself is not sufficient to remove the phase problem. To see this we consider the phase of $\langle\Psi_T|\phi'(\mathbf{x}-\bar{\mathbf{x}})\rangle/\langle\Psi_T|\phi\rangle$, which we denote by $\Delta\theta$. In general, $\Delta\theta \sim \mathcal{O}(-\mathbf{x}\mathrm{Im}(\bar{\mathbf{x}}))$ is non-zero. This means that the walkers will undergo a random walk in the complex plane. At large β they will therefore populate the complex plane symmetrically, independent of their initial positions. This is illustrated in the right panel of Fig. 4, which shows $\langle\Psi_T|\phi\rangle$ for a three-dimensional jellium model with two electrons at $r_s = 10$ for a total projection time of $\beta = 250$ (taken from Zhang 2013). The random walk is "rotationally invariant" in the complex plane, resulting in a vanishing signal-to-noise ratio asymptotically, even though the walkers are all real initially with $\langle\Psi_T|\phi^{(0)}\rangle = 1$. An alternative but related way to state the problem is that, despite the divergence of $\bar{\mathbf{x}}$, the buildup of a finite density at the origin of the complex plane cannot be prevented, unlike in the one-dimensional situation (real $\langle\Psi_0|\phi\rangle$, sign problem). Near the origin the local energy E_L diverges, which causes diverging fluctuations in the weights of walkers when the density does not vanish.

Thus the second ingredient of the constraint for the phase problem is to project the random walk back to "one-dimension." This is done by reducing the weight of the walker in each step by the angular deviation of the overlap in the complex plane:

$$w_{\phi'} \to w_{\phi'} \max\{0, \cos(\Delta\theta)\}\,. \tag{40}$$

A prerequisite for this approximation to work well is the importance-sampling transformation, which has eliminated the leading order in the overall phase of $|\phi\rangle$ in the propagator in Eq. (35). Given the transformation, several alternative forms to the projection in Eq. (40) were found to give similar accuracy (Zhang and Krakauer 2003; Zhang et al. 2005; Purwanto and Zhang 2005; Zhang 2013).

We can now summarize each step in the constrained path AFQMC formalism as follows. For each random walker $|\phi\rangle$ in the current population $\{|\phi\rangle, w_\phi\}$,

(a) Sample $\mathbf{x}$ and propagate the walker to $|\phi'\rangle$

$$|\phi\rangle \to |\phi'\rangle = \exp\left[-\frac{\Delta\tau\hat{H}_1}{2}\right] \exp\left[(\mathbf{x}-\bar{\mathbf{v}})\cdot\hat{\mathbf{v}}\right] \exp\left[-\frac{\Delta\tau\hat{H}_1}{2}\right] |\phi\rangle, \tag{41}$$

(b) Update the weight of the walker

$$w_\phi \to w_{\phi'} = w_\phi \exp\Big[-\Delta\tau \cdot \mathrm{Re}\Big(E_L(\phi') + E_L(\phi)\Big)/2\Big] \cdot \max\{0, \cos(\Delta\theta)\}\,. \tag{42}$$

Walkers so generated represent the ground-state wave function with importance sampling, in the sense of Eq. (32).

For additional technical details, we refer the reader to Zhang (2013) and Motta and Zhang (2018), and references therein, for example, re-orthogonalization procedures (White et al. 1989; Zhang 2003) to stabilize the walkers against numerical roundoff errors during the propagation, population control (Umrigar et al. 1993; Zhang et al. 1997) to regularize the branching process, a hybrid alternative (Purwanto et al. 2009a) to the local energy formalism in Eq. (36) to reduce computational cost in evaluating E_l, correlated sampling (Shee et al. 2017), constraint release (Shi and Zhang 2013), etc.

3.3 Back-Propagation for Observables and Correlation Functions

To calculate a correlation function or the expectation value of an observable which does not commute with the Hamiltonian, the mixed estimate in Eq.(15) is biased, and the full estimator in Eq. (14) needs to be computed. In the path-integral form in Eq. (27), this is straightforward. With the open-ended random walks, however, it is slightly more involved. A back-propagation (BP) technique (Zhang et al. 1997; Purwanto and Zhang 2004; Motta and Zhang 2017) is employed.

The idea of the BP is to create two coupled populations to represent the bra and ket in Eq. (14), respectively. Because the population in the random walk is importance-sampled, two independent populations which are uncoupled would lead to large fluctuations in the estimator after the importance functions have been "undone" (Purwanto and Zhang 2004). In BP, we choose an iteration n and store the entire population $\{\,|\phi_k^{(n)}\rangle,\, w_k^{(n)}\,\}$, where k labels the walker in the population. As the random walk proceeds from n, we keep track of the following two items for each new walker: (1) the sampled auxiliary-field values that led to the new walker from its parent walker and (2) an integer label that identifies the parent. After an additional m iterations, we carry out the back-propagation: For each walker l in the $(n+m)$-th (current) population, we initiate a determinant $\langle\psi_T|$ and act on it with the corresponding propagators but taken in reverse order. The m successive propagators are constructed from the items stored between steps $n+m$ and n, with $\exp(-\Delta\tau\hat{H}_1/2)$ inserted where necessary. The resulting determinants $\langle\bar{\phi}_l^{(m)}|$ are combined with its parent from iteration n, $|\phi_k^{(n)}\rangle$, to compute $\langle\mathcal{O}\rangle_{\mathrm{BP}}$, where k is the index of the walker at step n from which walker l at step $(n+m)$ descended.

In molecular systems, an improvement over the standard procedure has been proposed (Motta and Zhang 2017). The approach, called back-propagation with path restoration (BP-PRes), allows one to "undo" some of the effect of the constraint in

the forward direction (the cos projection and the omission of the phase in E_l in the weight). This reduced the effect of the constraint, which is applied in the forward direction and does not preserve reversal symmetry in imaginary time. With these advances, accurate observables and atomic forces have been obtained in molecules, paving the way for geometry optimization and ab initio molecular dynamics with AFQMC.

Another recent development in methodology is the computation of imaginary-time correlation functions and excitations. The techniques (Vitali et al. 2016), which have been applied in model systems and ultracold atoms so far, are directly applicable to real materials.

4 Illustrative Results

The AFQMC method has been applied to lattice models, realistic solids (using plane-wave basis and pseudo potentials), molecular systems (using Gaussian basis sets), and downfolded model Hamiltonians of real materials (using DFT orbitals as basis sets). The method is just coming into form, and rapid advances in algorithmic development and in applications are ongoing. We briefly mention a few examples here to provide a flavor of how it has been applied to date to tackle problems of electron correlations in materials.

For lattice models, most of the applications involve "only" a sign problem, because of the short-range nature of the interaction. Here the constraint has no θ projection and reduces to a sign constraint. A large body of results exist, including recent benchmark results (LeBlanc et al. 2015). Systems of $\mathcal{O}(1000)$ electrons have been treated quite routinely. The AFQMC method has demonstrated excellent capabilities and accuracy, illustrating its potential as a general many-body computational paradigm. A key recent development (Qin et al. 2016) is to use the density or density matrix computed from AFQMC as a feedback into a mean-field calculation. The trial wave function $|\Psi_T\rangle$ obtained from the mean-field is then fed back into the AFQMC as a constraint, and a self-consistent constraining condition is achieved. This has led to further improvement in the accuracy and robustness of the calculation (Qin et al. 2016; Zheng et al. 2017).

For molecular systems, a recent review article is available (Motta and Zhang 2018) which describes in more detail the application of AFQMC in quantum chemistry. The formulation of AFQMC with Gaussian basis sets has been extremely valuable. Direct comparisons can be made with high-level QC results, which have provided valuable benchmark information and have been crucial in gauging the AFQMC method as a general approach. Figure 5 illustrates the results on molecules using both plane-wave plus pseudopotentials and Gaussian basis sets. In these calculations we have operated largely in an automated mode, inputting only the DFT or HF solutions as $|\Psi_T\rangle$. This illustrates a potential mode of operation for AFQMC as a "post-processing" approach for molecules and solids where additional accuracy is desired beyond standard DFT.

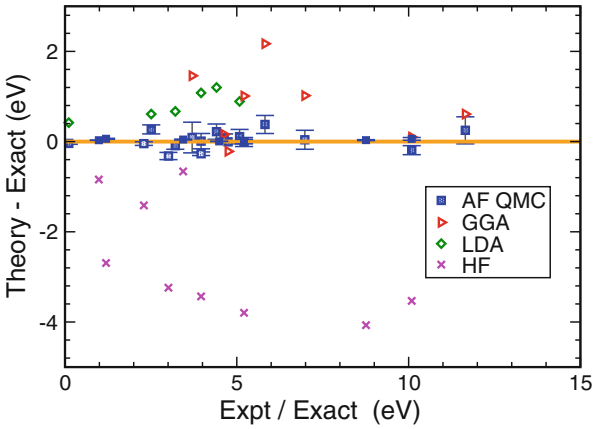

Fig. 5 Calculated binding energies of molecules compared with experimental values. (Taken from Zhang (2013); Esler et al. 2008). The discrepancy between theory and experiment is plotted. Included are *sp*-bonded molecules, first- and second-row post-*d* elements, and transition metal oxides. Several different forms of the AFQMC calculations were tested, including all-electron Gaussian basis sets, Gaussian basis with effective-core potentials, and plane wave with pseudopotential. The AFQMC is fed a trial wave function to start, which is taken directly from DFT [with either LDA or the generalized-gradient approximation (GGA) functionals] or HF. The corresponding DFT or HF results are also shown. As can be readily observed, the AFQMC results are in excellent agreement with experiment and significantly improve upon the values from DFT and HF

A benchmark study (Motta et al. 2017) was recently carried out involving a large set of modern many-body methods. AFQMC was among the methods included; consistent with previous findings, the accuracy of AFQMC is found to be comparable to CCSD(T), the gold standard in chemistry (Bartlett and Musiał 2007; Crawford and Schaefer 2000), near equilibrium geometry. For bond breaking, AFQMC was able to maintain systematic accuracy. Large basis sets and system sizes were reached and an accurate equation of state was obtained.

The AFQMC method can be used to study excited states. Excited states distinguished by different symmetry from the ground state can be computed in a manner similar to the ground state. For other excited states, prevention of collapse into the ground state and control of the fermion sign/phase problem are accomplished by a constraint using an excited state trial wave function (Purwanto et al. 2009b). An additional orthogonalization constraint is formulated to use virtual orbitals in solids for band structure calculations (Ma et al. 2013). These constraints are not as "clean" or rigorous as that for the ground state. Use of improved trial wave functions (e.g., multi-determinant $|\Psi_T\rangle$ in molecules) and the imposition of symmetry properties (Shi and Zhang 2013) often lead to improved results. Tests in the challenging case of the C_2 molecule yielded spectroscopic constants in excellent agreement with experiment (Purwanto et al. 2009b). In Fig. 6 results from an application in solids are shown for the diamond band structure and for the fundamental band gap in wurtzite ZnO (Ma et al. 2013).

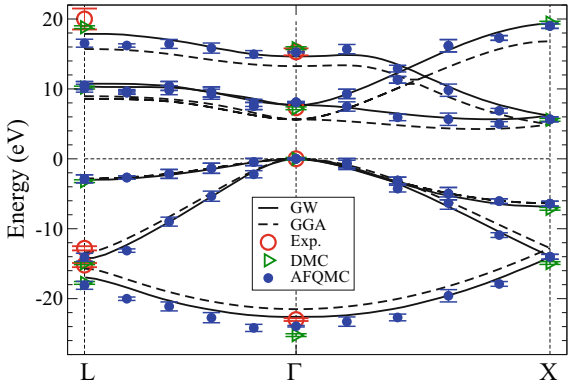

	Δ_{gap} (eV)
GGA	0.77
Hybrid	3.32, 2.90
LDA+U	1.0
GW	3.4, 3.6, 2.56
AFQMC	3.26(16)
expt.	3.30, 3.44, 3.57

Fig. 6 Computation of excitations and many-body quasiparticle band structures. (Taken from Ma et al. 2013). The figure presents results on the band gap in diamond. Blue is AFQMC results; GW and DFT band structures are plotted by solid and dashed lines, respectively. Diffusion Monte Carlo (DMC) results at high symmetry points Γ, X, and L are indicated by green triangles. Experimental values are shown as red circles. The table shows the calculated fundamental band gap of wurtzite ZnO, compared with experiment (and three DFT-based methods and GW)

Plane-wave calculations in AFQMC can be built on standard plane-wave technologies in DFT calculations, as we have outlined. Norm-conserving pseudopotentials, including multiple-projector pseudopotentials, can be implemented straightforwardly (Ma et al. 2017). In order to reduce the cost of full plane-wave AFQMC calculations, a downfolding approach (Ma et al. 2015) has been developed. The idea is to use Kohn-Sham orbitals (occupied and virtual) as basis sets. The approach is illustrated in Fig. 7. The size of the basis set in the largest calculation on the right, after downfolding, is more than an order of magnitude smaller than the total number of plane waves, leading to large savings in the AFQMC computation.

Figure 8 illustrates an application of AFQMC to the adsorption of Co atoms on graphene. The goal of the study was to determine the stability and magnetic state of the Co adatom as a function of its distance from the graphene sheet. The sensitivity and complexity of the energetics requires a correlated treatment. In addition to serving as a useful benchmark, the computed results provided an explanation for experimental results with Co on free-standing graphene (Virgus et al. 2014). The AFQMC calculation was performed by embedding it in a DFT calculation to extend length scales, as illustrated on the right. After the DFT is performed, a many-body Hamiltonian is generated, using a procedure similar to that of producing a frozen-core Hamiltonian (Purwanto et al. 2013), except the "core" here is actually the "outer" region indicated on the right. (Orbital localization procedures are applied as needed.) The resulting Hamiltonian, which describes the region inside the shaded circle embedded in the environment of the outer region whose orbitals are frozen, is then treated by AFQMC. From a QC perspective, this approach can also be viewed as casting AFQMC as a general "solver' for a (very large) active space (Motta and Zhang 2018).

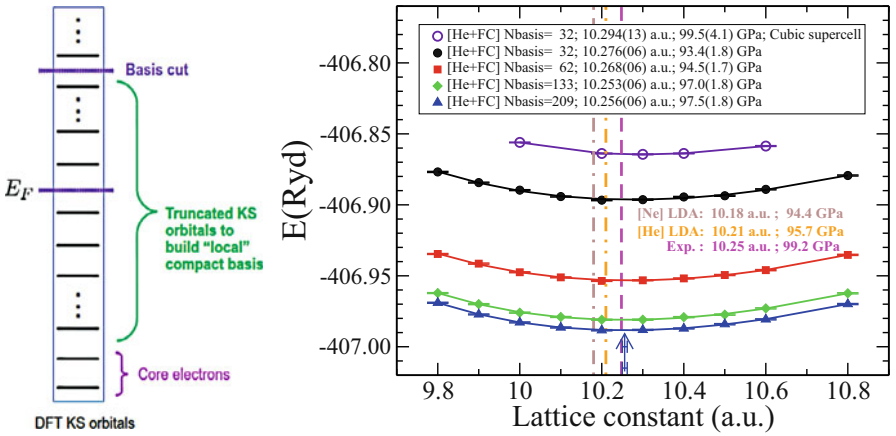

Fig. 7 Pseudopotential-free calculations in solids, and a simple "down-folding" approach to generate realistic model Hamiltonians. The **left panel** illustrates a scheme to use Kohn-Sham (KS) orbitals obtained from a DFT calculation as basis set for AFQMC. The DFT is performed with a plane-wave basis using a helium-core. Keeping all the KS orbitals, including virtual orbitals, below a certain cutoff ("Basis cut"), we compute the matrix elements with these orbitals as basis, to obtain a many-body Hamiltonian, which is then fed into the AFQMC. In the AFQMC, the KS orbitals corresponding to the neon-core are frozen (Purwanto et al. 2013). In the **right panel**, the calculated equation of state (Ma et al. 2015) is shown for a sequence of "Basis cut" values. The calculated equilibrium lattice constant and bulk modulus are in excellent agreement with experiment

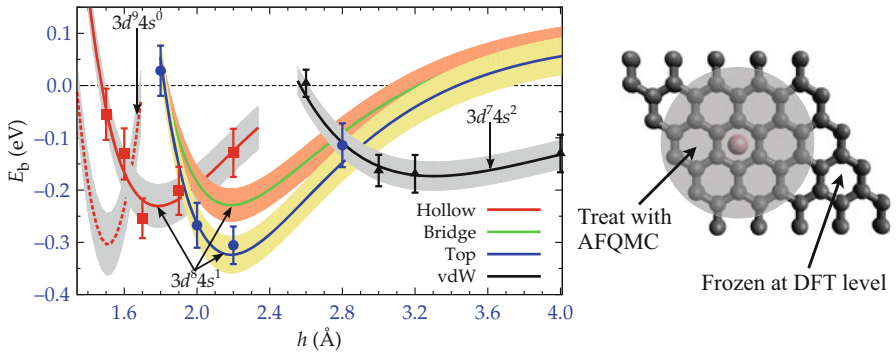

Fig. 8 Co-adsorption on graphene and embedding AFQMC within DFT. The figure (Taken from Virgus et al. 2014) shows computed binding energy of Co on graphene, as a function of the distance h between the Co atom and the graphene plane. Squares, diamonds, circles, and triangles correspond to hollow (H, as illustrated on the right), bridge (B), and top (T) sites and the van der Waals region, respectively. The dashed line indicates the low-spin H site (open squares). Shaded areas are one-σ estimates of uncertainties, including the statistical errors in AFQMC. The right illustrates the embedding scheme for these calculations. The "inner" region with Co and the C atoms inside the circle are treated by AFQMC, with the "outer" region providing a frozen environment

5 Summary and Outlook

In this chapter, we have described a general computational framework for many-body calculations which combines a field-theoretic description with stochastic sampling. The approach, referred to as auxiliary-field quantum Monte Carlo (AFQMC), is based on a stochastic superposition of DFT-like calculations. We have shown how the framework can be applied to carry out ab initio electronic structure calculations. As mentioned, some additional references for further details include a set of lecture notes (Zhang 2013) (on which some of the sections in this chapter are based), a pedagogical code for lattice models written in Matlab (Nguyen et al. 2014) and a review on molecular systems (Motta and Zhang 2018).

The AFQMC approach has been applied in both condensed matter physics and quantum chemistry. It has been implemented with both plane waves/pseudopotentials and with Gaussian basis sets. We have discussed both types of calculations, as well as a combination which uses Kohn-Sham orbitals generated from plane-wave DFT as a basis to downfold the Hamiltonian for a solid. In all of these, as well as in many applications to lattice models for strong electron correlation and for ultracold atom systems, AFQMC has shown strong promise with its scalability (with system size and with parallel computing platforms), capability (total energy computation and beyond), and accuracy.

The AFQMC method has low-polynomial (cubic) scaling with system size, by using Monte Carlo sampling to treat the exponential growth of the Hilbert space. It samples the many-body ground state by a linear combination of non-orthogonal Slater determinants. The connection with independent-electron calculations, as we have highlighted, makes it straightforward to build AFQMC as a framework on top of traditional DFT or HF calculations and take advantage of the many existing technical machineries developed over the past few decades in materials modeling.

Recent developments in the computation of atomic forces and geometry optimization, and the treatment of spin-orbit coupling and general magnetic order, are manifestations of this connection. They significantly enhance the capability of stochastic methods for electronic structure. Similarly, the formulation for superconducting Hamiltonians and for embedding AFQMC in independent-electron calculations to extend length scales will broaden the reach in materials computation.

The AFQMC is approximate, because of the constraint to control the sign/phase problem. A major focus during the development of the framework has been to systematically test (and improve) the accuracy of AFQMC. A large database has now been accumulated, thanks in part to the major many-electron benchmark initiatives recently. The accuracy that can be achieved by AFQMC with its present stage of development is such that many applications are now within reach in materials modeling. A variety of new developments are possible and currently being pursued.

The structure of the open-ended random walk, as illustrated in Fig. 3, makes AFQMC ideally suited for modern high-performance computing platforms, with

exceptional capacity for parallel scaling. The rapid growth of high-performance computing resources will thus provide a strong boost to the application of AFQMC in the study of molecules and solids.

The development of AFQMC is entering an exciting new phase. A large number of possible directions can be pursued, including many opportunities for algorithmic improvements and speedups. These will be spurred forward and stimulated by growth in applications, which we hope will in turn allow more rapid realization of a general many-body computational framework for materials.

Acknowledgments I thank the many colleagues and outstanding students and postdocs whose contributions to the work discussed here are invaluable, among whom I would especially like to mention W. Al-Saidi, H. Krakauer, F. Ma, M. Motta, W. Purwanto, and H. Shi. Support from the National Science Foundation (NSF), the Simons Foundation, and the Department of Energy (DOE) is gratefully acknowledged. Computing was done via XSEDE supported by NSF, on the Oak Ridge Leadership Computing Facilities, and on the HPC facilities at William & Mary.

References

Al-Saidi WA, Zhang S, Krakauer H (2006) Auxiliary-field quantum Monte Carlo calculations of molecular systems with a Gaussian basis. J Chem Phys 124(22):224101

Al-Saidi WA, Krakauer H, Zhang S (2007) A study of H + H_2 and several H-bonded molecules by phaseless auxiliary-field quantum Monte Carlo with plane wave and Gaussian basis sets. J Chem Phys 126(19):194105. https://doi.org/10.1063/1.2735296

Aquilante F, De Vico L, Ferre N, Ghigo G, Malmqvist P, Neograd y P, Pedersen T, Pitonak M, Reiher M, Roos B, Serrano-Andres L, Urban M, Veryazov V, Lindh R (2010) J Comput Chem 31(1):224–247. https://doi.org/10.1002/jcc.21318. The information about affiliations in this record was updated in December 2015. The record was previously connected to the following departments: Theoretical Chemistry (S) (011001039)

Baer R, Head-Gordon M, Neuhauser D (1998) Shifted-contour auxiliary field Monte Carlo for ab initio electronic structure: straddling the sign problem. J Chem Phys 109(15):6219–6226. https://doi.org/10.1063/1.477300

Bartlett RJ, MusiałM (2007) Coupled-cluster theory in quantum chemistry. Rev Mod Phys 79(1):291. https://doi.org/10.1103/RevModPhys.79.291

Blankenbecler R, Scalapino DJ, Sugar RL (1981) Monte Carlo calculations of coupled Boson-Fermion systems. I. Phys Rev D 24:2278

Booth GH, Thom AJW, Alavi A (2009) Fermion Monte Carlo without fixed nodes: a game of life, death, and annihilation in slater determinant space. J Chem Phys 131(5):054106. https://doi.org/10.1063/1.3193710

Car R, Parrinello M (1985) Unified approach for molecular dynamics and density functional theory. Phys Rev Lett 55:2471

Carlson J, Gandolfi S, Schmidt KE, Zhang S (2011) Auxiliary-field quantum Monte Carlo method for strongly paired fermions. Phys Rev A 84:061602. https://doi.org/10.1103/PhysRevA.84.061602

Ceperley DM (1995) Path integrals in the theory of condensed helium. Rev Mod Phys 67:279, and references therein

Crawford TD, Schaefer HF III (2000) An introduction to coupled cluster theory for computational chemists. Rev Comput Chem 14:33–136

Diedrich DL, Anderson JB (1992) An accurate quantum monte carlo calculation of the barrier height for the reaction $h + h_2 \rightarrow h_2 + h$. Science 258(5083):786–788. https://doi.org/10.1126/science.258.5083.786, http://science.sciencemag.org/content/258/5083/786.full.pdf

Esler KP, Kim J, Ceperley DM, Purwanto W, Walter EJ, Krakauer H, Zhang S, Kent PRC, Hennig RG, Umrigar C, Bajdich M, Kolorenc J, Mitas L, Srinivasan A (2008) Quantum Monte Carlo algorithms for electronic structure at the petascale; the Endstation project. J Phys Conf Ser 125:012057 (15pp). http://stacks.iop.org/1742-6596/125/012057

Fahy SB, Hamann DR (1990) Positive-projection Monte Carlo simulation: a new variational approach to strongly interacting fermion systems. Phys Rev Lett 65: 3437

Foulkes WMC, Mitas L, Needs RJ, Rajagopal G (2001) Quantum Monte Carlo simulations of solids. Rev Mod Phys 73:33, and references therein

Hamann DR, Fahy SB (1990) Energy measurement in auxiliary-field many-electron calculations. Phys Rev B 41(16):11352

Kalos MH, Whitlock PA (1986) Monte Carlo methods, vol I. Wiley, New York

Kalos MH, Levesque D, Verlet L (1974) Helium at zero temperature with hard-sphere and other forces. Phys Rev A 9:2178

Koch H, de Merás AS, Pedersen TB (2003) Reduced scaling in electronic structure calculations using Cholesky decompositions. J Chem Phys 118(21):9481–9484. https://doi.org/10.1063/1.1578621

Kohn W (1999) Nobel lecture: Electronic structure of matter – wave functions and density functionals. Rev Mod Phys 71:1253, and references therein

LeBlanc JPF, Antipov AE, Becca F, Bulik IW, Chan GKL, Chung CM, Deng Y, Ferrero M, Henderson TM, Jiménez-Hoyos CA, Kozik E, Liu XW, Millis AJ, Prokof'ev NV, Qin M, Scuseria GE, Shi H, Svistunov BV, Tocchio LF, Tupitsyn IS, White SR, Zhang S, Zheng BX, Zhu Z, Gull E (2015) Solutions of the two-dimensional hubbard model: benchmarks and results from a wide range of numerical algorithms. Phys Rev X 5:041041. https://doi.org/10.1103/PhysRevX.5.041041

Loh EY Jr, Gubernatis JE, Scalettar RT, White SR, Scalapino DJ, Sugar R (1990) Sign problem in the numerical simulation of many-electron systems. Phys Rev B 41:9301

Ma F, Zhang S, Krakauer H (2013) Excited state calculations in solids by auxiliary-field quantum Monte Carlo. New J 15:093017. https://doi.org/10.1088/1367-2630/15/9/093017

Ma F, Purwanto W, Zhang S, Krakauer H (2015) Quantum Monte Carlo calculations in solids with downfolded hamiltonians. Phys Rev Lett 114:226401. https://doi.org/10.1103/PhysRevLett.114.226401

Ma F, Zhang S, Krakauer H (2017) Auxiliary-field quantum Monte Carlo calculations with multiple-projector pseudopotentials. Phys Rev B 95:165103. https://doi.org/10.1103/PhysRevB.95.165103

Martin RM (2004) Electronic structure: basic theory and practical methods. Cambridge University Press, Cambridge

Moskowitz JW, Schmidt KE, Lee MA, Kalos MH (1982) A new look at correlation energy in atomic and molecular systems. II. The application of the Green's function Monte Carlo method to LiH. J Chem Phys 77:349

Motta M, Zhang S (2017) Computation of ground-state properties in molecular systems: back-propagation with auxiliary-field quantum Monte Carlo. J Chem Theory Comput 13(11):5367–5378. https://doi.org/10.1021/acs.jctc.7b00730, PMID:29053270

Motta M, Zhang S (2018, in press) Ab initio computations of molecular systems by the auxiliary-field quantum Monte Carlo method. WIREs Comput Mol Sci. https://doi.org/10.1002/wcms.1364

Motta M, Ceperley DM, Chan GKL, Gomez JA, Gull E, Guo S, Jiménez-Hoyos CA, Lan TN, Li J, Ma F, Millis AJ, Prokof'ev NV, Ray U, Scuseria GE, Sorella S, Stoudenmire EM, Sun Q, Tupitsyn IS, White SR, Zgid D, Zhang S (2017) Towards the solution of the many-electron

problem in real materials: equation of state of the hydrogen chain with state-of-the-art many-body methods. Phys Rev X 7:031059. https://doi.org/10.1103/PhysRevX.7.031059
Negele JW, Orland H (1998) Quantum many-particle systems. Advanced book classics. Perseus Books, Reading
Nguyen H, Shi H, Xu J, Zhang S (2014) CPMC-lab: a matlab package for constrained path Monte Carlo calculations. Comput Phys Commun 185(12):3344–3357. https://doi.org/10.1016/j.cpc.2014.08.003, http://www.sciencedirect.com/science/article/pii/S0010465514002707
Purwanto W, Zhang S (2004) Quantum Monte Carlo method for the ground state of many-boson systems. Phys Rev E 70:056702
Purwanto W, Zhang S (2005) Correlation effects in the ground state of trapped atomic bose gases. Phys Rev A 72(5):053610
Purwanto W, Krakauer H, Zhang S (2009a) Pressure-induced diamond to β -tin transition in bulk silicon: a quantum Monte Carlo study. Phys Rev B 80(21):214116. https://doi.org/10.1103/PhysRevB.80.214116
Purwanto W, Zhang S, Krakauer H (2009b) Excited state calculations using phaseless auxiliary-field quantum Monte Carlo: potential energy curves of low-lying C_2 singlet states. J Chem Phys 130(9):094107. https://doi.org/10.1063/1.3077920
Purwanto W, Krakauer H, Virgus Y, Zhang S (2011) Assessing weak hydrogen binding on Ca^+ centers: an accurate many-body study with large basis sets. J Chem Phys 135:164105
Purwanto W, Zhang S, Krakauer H (2013) Frozen-orbital and downfolding calculations with auxiliary-field quantum Monte Carlo. J Chem Theory Comput. https://doi.org/10.1021/ct4006486
Qin M, Shi H, Zhang S (2016) Coupling quantum Monte Carlo and independent-particle calculations: self-consistent constraint for the sign problem based on the density or the density matrix. Phys Rev B 94:235119. https://doi.org/10.1103/PhysRevB.94.235119
Rosenberg P, Shi H, Zhang S (2017) Accurate computations of Rashba spin-orbit coupling in interacting systems: from the Fermi gas to real materials. J Phys Chem Solids. https://doi.org/10.1016/j.jpcs.2017.12.026, 1710.00887
Schmidt KE, Kalos MH (1984) Few- and many-Fermion problems. In: Binder K (ed) Applications of the Monte Carlo method in statistical physics. Springer, Heidelberg
Shee J, Zhang S, Reichman DR, Friesner RA (2017) Chemical transformations approaching chemical accuracy via correlated sampling in auxiliary-field quantum Monte Carlo. J Chem Theory Comput 13(6):2667–2680. https://doi.org/10.1021/acs.jctc.7b00224, PMID: 28481546
Shi H, Zhang S (2013) Symmetry in auxiliary-field quantum Monte Carlo calculations. Phys Rev B 88:125132
Shi H, Zhang S (2016) Infinite variance in fermion quantum Monte Carlo calculations. Phys Rev E 93:033303. https://doi.org/10.1103/PhysRevE.93.033303
Shi H, Zhang S (2017) Many-body computations by stochastic sampling in Hartree-Fock-Bogoliubov space. Phys Rev B 95:045144. https://doi.org/10.1103/PhysRevB.95.045144
Sorella S, Baroni S, Car R, Parrinello M (1989) A novel technique for the simulation of interacting fermion systems. Europhys Lett 8:663
Suewattana M, Purwanto W, Zhang S, Krakauer H, Walter EJ (2007) Phaseless auxiliary-field quantum Monte Carlo calculations with plane waves and pseudopotentials: applications to atoms and molecules. Phys Rev B (Condensed Matter Mater Phys) 75(24):245123. https://doi.org/10.1103/PhysRevB.75.245123
Sugiyama G, Koonin SE (1986) Auxiliary field Monte-Carlo for quantum many-body ground states. Ann Phys (NY) 168:1
Szabo A, Ostlund N (1989) Modern quantum chemistry. McGraw-Hill, New York
Umrigar CJ, Nightingale MP, Runge KJ (1993) A diffusion Monte Carlo algorithm with very small time-step errors. J Chem Phys 99(4):2865
Virgus Y, Purwanto W, Krakauer H, Zhang S (2014) Stability, energetics, and magnetic states of cobalt adatoms on graphene. Phys Rev Lett 113:175502. https://doi.org/10.1103/PhysRevLett.113.175502

Vitali E, Shi H, Qin M, Zhang S (2016) Computation of dynamical correlation functions for many-fermion systems with auxiliary-field quantum Monte Carlo. Phys Rev B 94:085140. https://doi.org/10.1103/PhysRevB.94.085140

Wei ZC, Wu C, Li Y, Zhang S, Xiang T (2016) Majorana positivity and the fermion sign problem of quantum Monte Carlo simulations. Phys Rev Lett 116:250601. https://doi.org/10.1103/PhysRevLett.116.250601

White SR, Scalapino DJ, Sugar RL, Loh EY, Gubernatis JE, Scalettar RT (1989) Numerical study of the two-dimensional Hubbard model. Phys Rev B 40(1):506

Zhang S (1999a) Constrained path Monte Carlo for fermions. In: Nightingale MP, Umrigar CJ (eds) Quantum Monte Carlo methods in physics and chemistry. Kluwer Academic Publishers, Dordrech, cond-mat/9909090

Zhang S (1999b) Finite-temperature Monte Carlo calculations for systems with fermions. Phys Rev Lett 83:2777

Zhang S (2003) Quantum Monte Carlo methods for strongly correlated fermions. In: Sénéchal D, Tremblay AM, Bourbonnais C (eds) Theoretical methods for strongly correlated electrons. CRM series in mathematical physics, and references therein. Springer, New York

Zhang S (2013) Auxiliary-Field quantum monte carlo for correlated electron systems. In: Pavarini E, Koch E, Schollwöck U (eds) Emergent phenomena in correlated matter: modeling and simulation, vol 3. Verlag des Forschungszentrum Jülich, Jülich

Zhang S, Ceperley DM (2008) Hartree-Fock ground state of the three-dimensional electron gas. Phys Rev Lett 100:236404

Zhang S, Kalos MH (1991) Exact Monte Carlo calculations for few-electron systems. Phys Rev Lett 67:3074

Zhang S, Krakauer H (2003) Quantum Monte Carlo method using phase-free random walks with Slater determinants. Phys Rev Lett 90:136401

Zhang S, Carlson J, Gubernatis JE (1997) Constrained path Monte Carlo method for fermion ground states. Phys Rev B 55:7464

Zhang S, Krakauer H, Al-Saidi WA, Suewattana M (2005) Quantum simulations of realistic systems by auxiliary fields. Comput Phys Commun 169:394

Zheng BX, Chung CM, Corboz P, Ehlers G, Qin MP, Noack RM, Shi H, White SR, Zhang S, Chan GKL (2017) Stripe order in the underdoped region of the two-dimensional Hubbard model. Science 358(6367):1155–1160. https://doi.org/10.1126/science.aam7127